ADVANCES IN ATMOSPHERIC SCIENCES, VOL. 34, JULY 2017, 859–876

• **Original Paper** •

Cloud Radiative Effects and Changes Simulated by the Coupled Model Intercomparison Project Phase 5 Models

Sun-Hee SHIN[1], Ok-Yeon KIM[1], Dongmin KIM[2], and Myong-In LEE[*2]

[1] *Climate Research Department, APEC Climate Center, Busan* 48058*, Republic of Korea*
[2] *School of Urban and Environmental Engineering, Ulsan National Institute of Science and Technology, Ulsan* 44919*, Republic of Korea*

(Received 8 April 2016; revised 14 February 2017; accepted 8 March 2017)

ABSTRACT

Using 32 CMIP5 (Coupled Model Intercomparison Project Phase 5) models, this study examines the veracity in the simulation of cloud amount and their radiative effects (CREs) in the historical run driven by observed external radiative forcing for 1850–2005, and their future changes in the RCP (Representative Concentration Pathway) 4.5 scenario runs for 2006–2100. Validation metrics for the historical run are designed to examine the accuracy in the representation of spatial patterns for climatological mean, and annual and interannual variations of clouds and CREs. The models show large spread in the simulation of cloud amounts, specifically in the low cloud amount. The observed relationship between cloud amount and the controlling large-scale environment are also reproduced diversely by various models. Based on the validation metrics, four models—ACCESS1.0, ACCESS1.3, HadGEM2-CC, and HadGEM2-ES—are selected as best models, and the average of the four models performs more skillfully than the multimodel ensemble average.

All models project global-mean SST warming at the increase of the greenhouse gases, but the magnitude varies across the simulations between 1 and 2 K, which is largely attributable to the difference in the change of cloud amount and distribution. The models that simulate more SST warming show a greater increase in the net CRE due to reduced low cloud and increased incoming shortwave radiation, particularly over the regions of marine boundary layer in the subtropics. Selected best-performing models project a significant reduction in global-mean cloud amount of about $-0.99\%\ \mathrm{K}^{-1}$ and net radiative warming of $0.46\ \mathrm{W\ m^{-2}\ K^{-1}}$, suggesting a role of positive feedback to global warming.

Key words: cloud radiative effects, cloud feedback, climate change, CMIP5

Citation: Shin, S.-H., O.-Y. Kim, D. Kim, and M.-I. Lee, 2017: Cloud radiative effects and changes simulated by the Coupled Model Intercomparison Project Phase 5 models. *Adv. Atmos. Sci.*, **34**(7), 859–876, doi: 10.1007/s00376-017-6089-3.

1. Introduction

A rapid increase in the concentration of greenhouse gases is one of the primary causes of the observed warming trend in the global mean surface temperature for the past hundred years (IPCC, 2013). Although state-of-the-art climate models are able to reproduce the warming trend unanimously with increasing greenhouse gases in their historical runs, there are considerable differences in the degree of warming across the various model simulations (IPCC, 2013). This is largely caused by the uncertainty in the interaction and feedback processes between clouds and the Earth's climate system (Soden and Held, 2006; Randall et al., 2007; Dufresne and Bony, 2008; Waliser et al., 2009; Andrews et al., 2012; Vial et al., 2013; Li et al., 2013 and references therein). This uncertainty also leads to huge differences among their projections of future climate in the next century (Bony and Dufresne, 2005; Stephens, 2005; Bony et al., 2006; Randall et al., 2006; Webb et al., 2006; Wyant et al., 2006; Clement et al., 2009). There still exists a large spread in the climate sensitivity, which is defined as the global-mean surface temperature change under a doubled concentration of atmospheric CO_2, simulated by current climate models, with a range from 1.9 to 4.4 K (Randall et al., 2007; Andrews et al., 2012; Vial et al., 2013). Using 11 global models participating in the Coupled Model Intercomparison Project Phase 5 (CMIP5) (Taylor et al., 2012), Vial et al. (2013) estimated that the cloud feedback, as the primary source of model uncertainty in future climate projections, is responsible for approximately 70% of the intermodel spread in the climate sensitivity.

Clouds exhibit high temporal and spatial variation with a variety of types. Considering a significant role of clouds in regulating Earth's radiation balance and temperature distribution, a comprehensive assessment of the simulated cloud variation in space and time with reliable observations is a first

* Corresponding author: Myong-In LEE
Email: milee@unist.ac.kr

necessary step to evaluate the model biases and uncertainties. This will help us to understand the dominant mechanisms from the analysis of the observed cloud variation, from which one can further identify the key source of problems in the models, such as in the response of the simulated cloud to sea surface temperature (SST) and large-scale atmospheric forcings. Several studies (e.g., Klein and Hartmann, 1993; Norris and Leovy, 1994; Wood and Hartmann, 2006) have focused on the large-scale environmental controls of cloud variation, especially with respect to low-level clouds. Those studies have shown that changes in large-scale dynamic and thermodynamic conditions can explain much of the cloud variability on daily to interannual time scales. Clement et al. (2009) examined the relationship between low clouds and large-scale meteorological conditions in the Coupled Model Intercomparison Project Phase 3 (CMIP3) model simulations. Their study suggested a positive feedback in the global warming, induced by low-level cloud changes, based on model simulations. In a CMIP5 model assessment, Vial et al. (2013) also indicated that simulated cloud feedbacks in the tropics, particularly over the regions where shallow cumulus and stratocumulus clouds prevail, are significantly different across models.

Zelinka et al. (2012a, 2012b) proposed a way to compute cloud feedback by using an ISCCP simulator-produced cloud fraction histogram, which is a function of cloud-top pressure and optical depth. Based on this method, they separately computed the cloud amount, altitude and optical depth feedbacks in the Cloud Feedback Model Intercomparison Project Phase 1 (CFMIP1), as a subset of CMIP3. This method allowed them to assess the relative roles of these processes in longwave, shortwave and net cloud feedback. Zelinka et al. (2013) also assessed the cloud response to rapid adjustments and feedbacks in models participating in CMIP5/CFMIP2. Klein et al. (2013) then extended their analysis to the comparison of the climatological annual cycle of cloud amount, cloud-top pressure and optical thickness between CFMIP1 and CFMIP2. They showed significant improvements in the simulation of optical depth in CFMIP2 compared to CFMIP1.

Though many evaluations in terms of CMIP5 model simulations of clouds have been carried out thus far, the diagnostics suggested in this study include more rigorous comparisons of cloud amount and associated large-scale variables. More specifically, this is one of the first and most extensive studies in which the cloud diagnostics in the latest model collection of CMIP5 are compared, and will therefore act as a reference for the next CMIP phase. In this study, we develop comprehensive evaluation metrics to carefully examine the modeled cloud variation and the feedback using the most recent 32 climate projection models in CMIP5. As suggested by Vial et al. (2013), local and remote physical processes controlling low-cloud variations in the tropical oceans need to be better understood using observations and model simulations in order to assess the relative reliability of the different model responses. The model validation metrics are designed for evaluating whether they represent the observed relationship between clouds and large-scale dynamic and thermodynamic variables. The metrics include: (1) the spatial distribution of the annual-mean cloud climatology; (2) the monthly variation of clouds; and (3) the interannual variation of clouds. Most of the metrics consist of global- and regional-mean coefficients of spatial pattern correlation and root-mean-squared errors between the observed and the simulated variables. Regarding the metric for the interannual variation of cloud, the approach of this study basically follows Clement et al. (2009) and Shin et al. (2014), who examined the relationship between low clouds and large-scale environmental conditions. Clement et al. (2009) proposed a method to test the realism of cloud simulation in current-generation climate models through the cloud-meteorology correlation test. They suggested that a larger number of climate models should be considered with regard to the relationships between cloud cover and regional meteorological conditions, to ensure greater confidence in the sign of the low-cloud feedback response to future changes in greenhouse gas concentrations. Based on quantitative and aggregated evaluation metrics, this study selects the best performing models and examines their cloud projections in the future with enhanced confidence in a warming climate. Section 2 describes the validation data and the CMIP5 models used in this study. The spatiotemporal variation of clouds simulated by the CMIP5 models is evaluated in section 3, from which the best and most reliable models that realistically reproduce observed cloud variations are selected. Section 4 describes the future climate changes in association with cloud radiative effects (CREs) according to the best models. In addition, section 5 discusses the transient trend of clouds and their impacts on climate. A summary and conclusions are given in section 6.

2. Models and validation

2.1. *Models*

The model simulation data are obtained from the CMIP5 multi-model data archive (http://cmip-pcmdi.llnl.gov/cmip5/index.html). This study uses two types of experiments: the historical runs (available from 1850 to 2005), and the Representative Concentration Pathways (RCP) 4.5 runs from 2006 to 2100. The historical runs are used to evaluate the degree to which the models are realistic and robust in simulating the cloud variations in the recent past. The RCP4.5 run is used to estimate the cloud feedback and uncertainties in the future climate projections. The historical run is driven by observed natural and anthropogenic greenhouse gas forcings in the past, whereas the RCP4.5 run is driven by the future scenario of radiative forcing induced by the increase in the concentrations of greenhouse gases. The latter is the central scenario of CMIP5, which assumes an increase in radiative forcing for the next century and stabilization at 4.5 W m^{-2} after 2100 (Taylor et al., 2012). Table 1 lists the model names, their institutions, atmospheric component horizontal resolutions, and ensemble member numbers, for the 32 models used in this study. Due to the difference in ensemble members, only one ensemble member for each model is chosen for a fair comparison. Similar to the observational data, each simulation dataset is interpolated onto the same 2.5° latitude ×2.5° longitude grid. In our analysis, the multimodel ensemble (MME) mean is defined as the simple arithmetic average of the model runs. As in the observation, the model climatology is defined as the average of 1984–2005.

In Table 1, seven models (CanESM2, GFDL-ESM2M, HadGEM2-CC, HadGEM2-ES, MIROC-ESM, MPI-ESM, and NorESM1-M) are Earth System Models, able to simulate the biogeochemical cycles of carbon across the oceans,

Table 1. Details of the CMIP5 models used in the study.

Index	Institution	Coupled model	AGCM resolution (Lon × Lat)	No. of ensemble members
1	Commonwealth Scientific and Industrial Research Organization and Bureau of Meteorology, Australia (CSIRO-BOM)	ACCESS1.0	1.875° × 1.25°	1
2	Commonwealth Scientific and Industrial Research Organization and Bureau of Meteorology, Australia (CSIRO-BOM)	ACCESS1.3	1.875° × 1.25°	1
3	Beijing Climate Center (BCC), China Meteorological Administration	BCC_CSM1.1	2.8125° × 2.8125°	1
4	Beijing Climate Center (BCC), China Meteorological Administration	BCC_CSM1.1(m)	1.125° × 1.125°	1
5	College of Global Change and Earth System Science, Beijing Normal University (BNU)	BNU-ESM	2.8125° × 2.8125°	1
6	Canadian Centre for Climate Modeling and Analysis (CCCma)	CanESM2	2.8125° × 2.8125°	1
7	National Center for Atmospheric Research (NCAR)	CCSM4	1.25° × 0.9375°	1
8	Centre National de Recherches Météorologiques/Centre Europeen de Recherche et Formation Avancees en Calcul Scientifique (CNRM-CERFACS)	CNRM-CM5	1.40625° × 1.40625°	4
9	Commonwealth Scientific and Industrial Research Organisation/Queensland Climate Change Centre of Excellence (CSIRO-QCCCE)	CSIRO Mk3.6.0	1.875° × 1.875°	1
10	LASG, Institute of Atmospheric Physics, Chinese Academy of Sciences and CESS, Tsinghua University (LASG-CESS)	FGOALS-g2	2.8125° × 2.8125°	4
11	LASG, Institute of Atmospheric Physics, Chinese Academy of Sciences and CESS, Tsinghua University (LASG-CESS)	FGOALS-s2	1.667° × 2.8125°	2
12	First Institute of Oceanography, SOA, China	FIO-ESM	2.8125° × 2.8125°	1
13	Geophysical Fluid Dynamics Laboratory (GFDL)	GFDL CM3	2.5° × 2°	1
14	Geophysical Fluid Dynamics Laboratory (GFDL)	GFDL-ESM2G	2.5° × 2°	1
15	Geophysical Fluid Dynamics Laboratory (GFDL)	GDDL-ESM2M	2.5° × 2°	1
16	NASA Goddard Institute for Space Studies (NASA GISS)	GISS-E2-H	2.5° × 2°	1
17	NASA Goddard Institute for Space Studies (NASA GISS)	GISS-E2-R	2.5° × 2°	1
18	Met Office Hadley Centre	HadCM3	1.875° × 1.24°	1
19	Met Office Hadley Centre	HadGEM2-CC	1.875° × 1.24°	3
20	Met Office Hadley Centre	HadGEM2-ES	1.875° × 1.24°	1
21	Institute for Numerical Mathematics (INM)	INM-CM4	2° × 1.5°	1
22	L'Institute Pierre-Simon Laplace (IPSL)	IPSL-CM5A-LR	3.75° × 1.875°	1
23	L'Institute Pierre-Simon Laplace (IPSL)	IPSL-CM5A-MR	2.5° × 1.258°	1
24	L'Institute Pierre-Simon Laplace (IPSL)	IPSL-CM5B-LR	3.75° × 1.875°	1
25	Atmosphere and Ocean Research Institute (University of Tokyo), National Institute for Environmental Studies, and Japan Agency for Marine-Earth Science and Technology (MIROC)	MIROC5	1.40625° × 1.40625°	1
26	Atmosphere and Ocean Research Institute (University of Tokyo), National Institute for Environmental Studies, and Japan Agency for Marine-Earth Science and Technology (MIROC)	MIROC-ESM	2.8125° × 2.8125°	1
27	Atmosphere and Ocean Research Institute (University of Tokyo), National Institute for Environmental Studies, and Japan Agency for Marine-Earth Science and Technology (MIROC)	MIROC-ESM-CHEM	2.8125° × 2.8125°	1
28	Max Planck Institute for Meteorology (MPI-M)	MPI-ESM-LR	1.875° × 1.875°	1
29	Max Planck Institute for Meteorology (MPI-M)	MPI-ESM-P	1.875° × 1.875°	1
30	Meteorological Research Institute (MRI)	MRI-CGCM3	1.125° × 2.25°	1
31	Norwegian Climate Centre (NCC)	NorESM1-M	2.5° × 1.875°	1
32	Norwegian Climate Centre (NCC)	NorESM1-ME	2.5° × 1.875°	1

atmosphere and terrestrial biosphere. Some of the models also include interactive aerosols, chemistry, and dynamic vegetation components (Taylor et al., 2012). Therefore, the CMIP5 models may have larger model spread and uncertainty in their responses than those of CMIP3 (Yeh et al., 2012). In addition, some of the models have a higher horizontal resolution. Further details and related papers on the models and experiments can be found at PCMDI [http://cmip-pcmdi.llnl.gov/cmip5/experiment_design.html; also see Taylor et al. (2012)].

2.2. *Validation*

For validation of the models, this study uses the long-term satellite observations from the adjusted cloud amount and radiative flux data of the International Satellite Cloud Climatology Project (ISCCP). These data were originally archived by the ISCCP (Rossow and Schiffer, 1999) but adjusted because of several artifacts in the original dataset. To remove the spurious long-term variability related to changes in satellite orbit, instrument calibration, and other factors, the adjustment has been applied in the original ISCCP D2 monthly-mean cloud product during 1984–2008. This adjustment has not altered the spatial structure of the long-term observed cloud climatology [more detailed information on the adjustment processes and a discussion is provided in Clement et al. (2009)]. Note that the adjusted ISCCP datasets are useful for investigating regional cloud changes because the long-term artificial trends have been removed. Shin et al. (2014) used the same data for the validation of CMIP3 models. Clement et al. (2009) compared these data with other sources of data such as COADS (Comprehensive Ocean Atmosphere Data Set) (Worley et al., 2005) and PATMOS-x (Pathfinder Atmosphere's Extended dataset) (Pavolonis et al., 2005), and found good agreement in the total and low-level cloud amounts over the Northeast Pacific (not shown). These data also show good consistency with MODIS (Platnick et al., 2003) in terms of the seasonal variation over major subtropical marine stratocumulus regions, which are the main regions of focus in this study (black box in Fig. 1).

The ISCCP radiative flux data are also adjusted and used for the analysis of CREs (or cloud radiative forcing), defined as the difference in radiative fluxes between cloudy and cloud-free conditions. Other large-scale variables used in the analysis include the HadISST v1.1 SST from the Hadley Centre reanalysis (Rayner et al., 2003) and the sea level pressure (SLP), vertical velocity, and surface winds from ERA-40 (Uppala et al., 2005). Using these data, the lower-tropospheric stability (LTS) is defined as the potential temperature difference between 700 hPa and the surface. All data are interpolated to a common 2.5° latitude ×2.5° longitude grid. As the ISCCP data are available from 1984, the observed climatology is defined as the average of 1984–2005.

In section 3, we calculate the seasonal variation of clouds and CREs as

$$\mathrm{SSD}=\sqrt{\frac{\sum_{n=1}^{N}(x_n-\bar{x})^2}{N-1}}\,,$$

where "seasonal variation" represents the seasonal standard deviation (SSD), N = 12 (months), x is the climatological monthly mean, and $\bar{x}$ is the annual and climatological mean. This value is used to define the amplitude of the annual cycle.

The interannual variability of the simulated clouds by various CGCMs is examined, which includes comparisons of the temporal correlation of cloud cover with large-scale variables such as SST, LTS and SLP. The correlation is calculated using monthly anomalies of each variable by removing long-term monthly averages for 22 years (1984–2005). As indicated, this is the period when the ISCCP cloud observations are available. As in Clement et al. (2009) and Shin et al. (2014), the model validation is conducted over the ocean grid points only for 60°S–60°N, which is done in order to better elucidate the variational mechanisms and the role of marine stratocumulus in the global radiation budget.

3. Evaluation of the historical runs

3.1. *Spatial distributions of clouds*

The observed and simulated cloud distributions are examined in Fig. 1, where the annual-mean total cloud amount (TCA), low cloud amount (LCA), and high cloud amount (HCA) are compared, separately. In the observations, the TCA is particularly large over the major tropical convective regions and the storm track regions over midlatitude oceans. These are in fact mostly accounted for by high clouds in the tropics and midlatitudes. In contrast, low clouds are most abundant in the subtropical oceans, particularly in the eastern basins. The western basins in general show the smallest amount of low cloud, where small trade wind cumuli are the predominant cloud type (Klein and Hartmann, 1993). Although the MME tends to underestimate the cloud amounts globally, it reproduces the observed patterns fairly well, including cloudy areas over the oceanic intertropical convergence zones and the regions of major storm tracks in the extratropical Pacific, in which high clouds are realistically simulated. However, the models have great difficulty in simulating realistic low cloud cover; specifically, they underestimate the low cloud over the eastern subtropical oceans.

Changes in the horizontal and vertical distribution of clouds affect the global radiation balance significantly. The impacts of clouds on Earth's radiation budget can be quantified by the CRE, which is defined as the radiative flux difference between clear conditions and all-sky conditions (Ramanathan et al., 1989; Hartmann et al., 2001). Climatological-mean patterns of the CRE are also analyzed in Fig. 1, for net, shortwave and longwave radiation, separately. The net CRE is the sum of the longwave CRE (LCRE: warming effect) and shortwave CRE (SCRE: cooling effect). The cooling effect of observed clouds is particularly evident over the eastern subtropical oceans, where low-level clouds are prevalent; whereas, it becomes weak over the warm pools in the western Pacific and the Indian Ocean. In the tropics, the SCRE and LCRE are both strong and nearly cancel each other out by strong greenhouse warming and high reflective

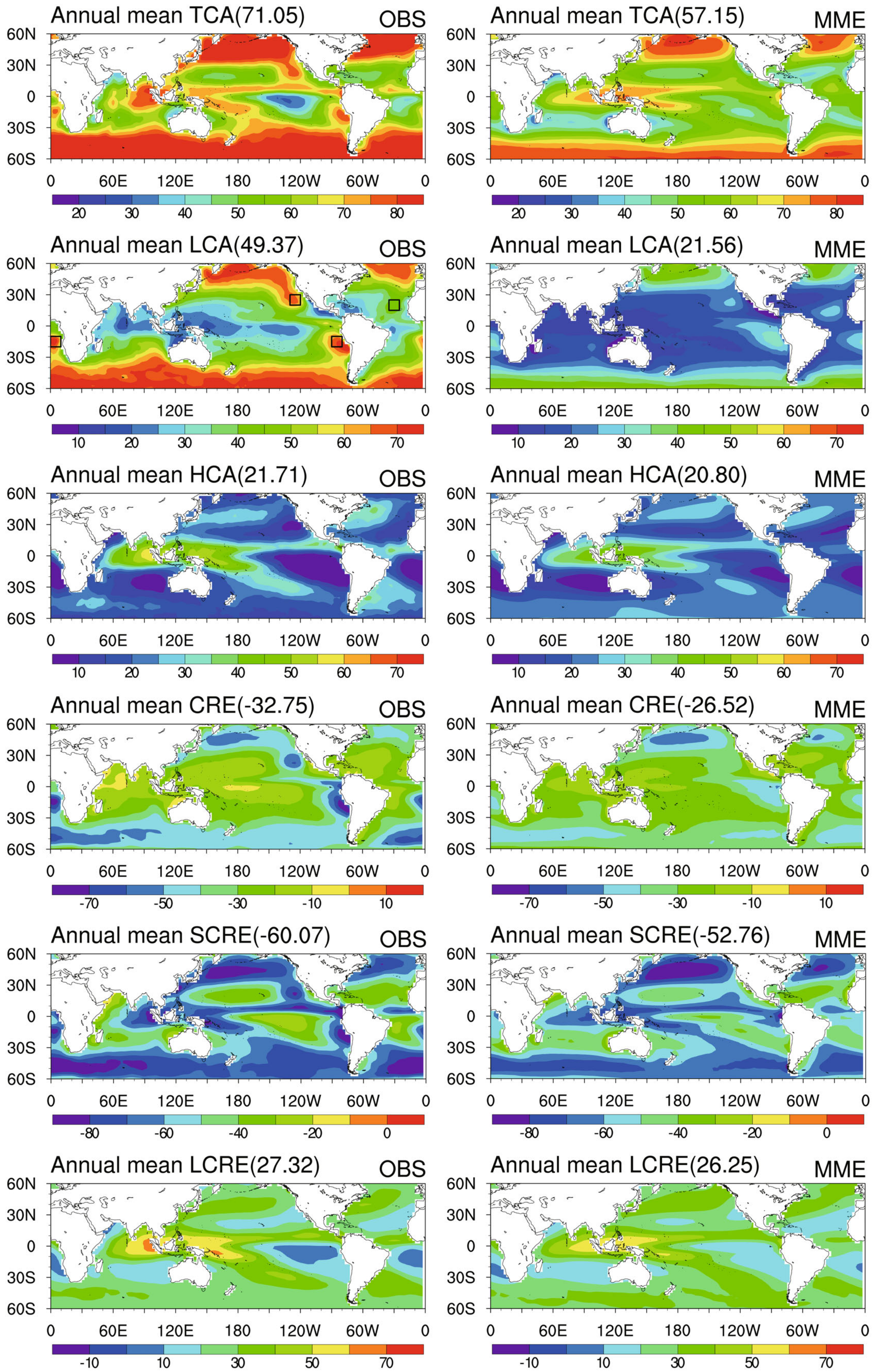

Fig. 1. Comparison of cloud climatology (1984–2005) between observations (ISCCP) and the MME of the 32 CGCMs for the TCA (%), LCA (%), HCA (%), net CRE (W m^{-2}), SCRE (W m^{-2}), and LCRE (W m^{-2}). Each number in parentheses is averaged value over the ocean area of 60°S–60°N (latitude) and 180°W–180°E (longitude). The black box indicate four low cloud regions defined in Fig. 9.

cooling by deep convective clouds. Although the MME captures the basic features of the geographical distribution of the CRE, it also shows some discrepancies. For example, both the SCRE and LCRE are underestimated over the Indo-Pacific warm pool region, where the amount of deep convective clouds is underestimated in the MME. The MME also fails to capture the large reflection by clouds in the eastern subtropical oceans due to the shortcomings of the model simulation for low clouds.

In terms of quantitatively measuring the simulation performance for annual–mean cloud, we compare the pattern correlation coefficients (PCCs) and normalized root–mean-square error (NRMSE) between the observation and the simulations from individual models and their MME over 60°S–60°N and 180°W–180°E (Fig. 2). The NRMSE is defined as the RMSE divided by the observed standard deviation, which is calculated with respect to the global mean. Figure 2 (left-hand panels) shows that the CMIP5 models can reproduce the observed HCA more realistically than the LCA. The wide spread of the PCC and NRMSE scores for the TCA is primarily caused by intermodel differences and poor simulations for low cloud. While the MME is better than any single model in the simulation of HCA, this is not the case for LCA. Figure 2 (right-hand panels) also presents the PCC and NRMSE scores for the CREs. In general, the models with higher PCCs tend to show smaller NRMSEs for all CREs. It is also interesting to note that the CREs represented by the MME exhibit better resemblance to the observed than any individual model simulation. The wide spread of the CRE, as shown by the PCC and NRMSE scores, across the models, is mostly due to intermodel differences in the SCRE caused by model deficiencies in low cloud simulation. To summarize the spatial pattern test for the annual-mean cloud amount and CREs, we define a good model group using the median value of models' PCCs and NRMSEs. The good model group, comprising ACCESS1.0, ACCESS1.3, CanESM2, GFDL-CM3, HadGEM2-CC, and HadGEM2-ES, shows a commonly larger PCC and smaller NRMSE in all variables compared to the other models.

3.2. *Monthly variation of cloud amount*

In Fig. 3, the amplitude of the annual cycle for TCA, LCA and HCA are compared between the ISCCP observation and the MME simulation, separately. Strong annual variation in TCA is found over the tropical eastern Pacific, Arabian Sea, Bay of Bengal, and the warm pool ocean to the north of Australia—mostly the deep convective regions. The observed cloud area shifts north and south according to the seasonal migration of ITCZs, which produces regions of strong seasonal variation straddling the equator. The annual variation of TCA is dominated by low cloud over the southeastern Pacific and southeastern Atlantic and high cloud related to the seasonal migration of ITCZs. The MME reproduces the major observed features, including the seasonal shifts of ITCZs over the western Pacific and seasonal variation of LCA over the subtropical eastern Pacific and Atlantic. However, the MME has difficulty in simulating realistic patterns of high cloud over the eastern Pacific and low cloud maxima over the South China Sea. Although the MME tends to greatly underestimate the amplitude of the seasonal cycle of cloud amount, it tends to capture the correct phase of the LCA and HCA variation over the eastern subtropical oceans and the ITCZ over the eastern Pacific, respectively (not shown).

Figure 4 compares the PCC and NRMSE scores for the annual cycles of cloud amounts and CREs. Again, the MME performs better than individual models in terms of the annual cycle of the amplitude of TCA and HCA, but not LCA. The MME is again better than individual models in terms of simulating the annual amplitude of CREs. Overall, ACCESS1.0, ACCESS1.3, HadGEM2-CC, and HadGEM2-ES produce better simulations both for the annual cycles of cloud amounts and the CREs.

3.3. *Interannual variation in cloud amount*

Next, we examine the relationship between SST and the three different types of cloud amount (TCA, LCA and HCA) for observations and model simulations, separately (Fig. 5). The covariability between the SST and cloud amount depends on the cloud type, even changing its sign. In most regions, the LCA correlates negatively with SST, apart from a weak positive correlation over some off-equatorial ocean regions and the equatorial Indian Ocean. Negative correlation is particularly pronounced over tropical convection regions, which is consistent with previous observation-based studies (Norris and Leovy, 1994; Wyant et al., 1997; Clement et al., 2009; Eastman et al., 2011). On the other hand, the HCA correlates positively with SST over the tropical convection regions, but elsewhere shows little correlation. The correlation pattern of TCA with SST is actually a superposition of the two patterns—one from the pattern of LCA dominated by negative correlations with SST over the subtropical oceans, and the other from the pattern of HCA dominated by positive correlations with SST over the tropical convection regions. The MME roughly reproduces the spatial pattern of the correlations between SST and TCA in the tropical convection regions and subtropical oceans. The strength of the positive correlation for HCA and the negative correlation for LCA are too weak over the SPCZ and warm pool regions and in the subtropical oceans, respectively. On the other hand, some individual models, such as ACCESS1.0, CCSM4, HadGEM2-CC, HadGEM2-ES, IPSL-CM5B-LR, and NorESM1-ME, reproduce the observed spatial pattern fairly well (not shown). The spatial extent and strength of the positive and negative correlations are best expressed, compared to observation, in ACCESS1.0, with maximum negative correlation of 0.4–0.6 over the subtropical marine area and maximum positive correlation of 0.6–0.8 over the equatorial central Pacific.

Figure 6 shows the correlation patterns of LTS with TCA, LCA and HCA, separately. While LCA correlates negatively with SST, it shows strong positive correlation with LTS. According to Klein and Hartmann (1993), low cloud variation is more closely correlated with low-level atmospheric stability variation, rather than with SST. Increasing SST tends

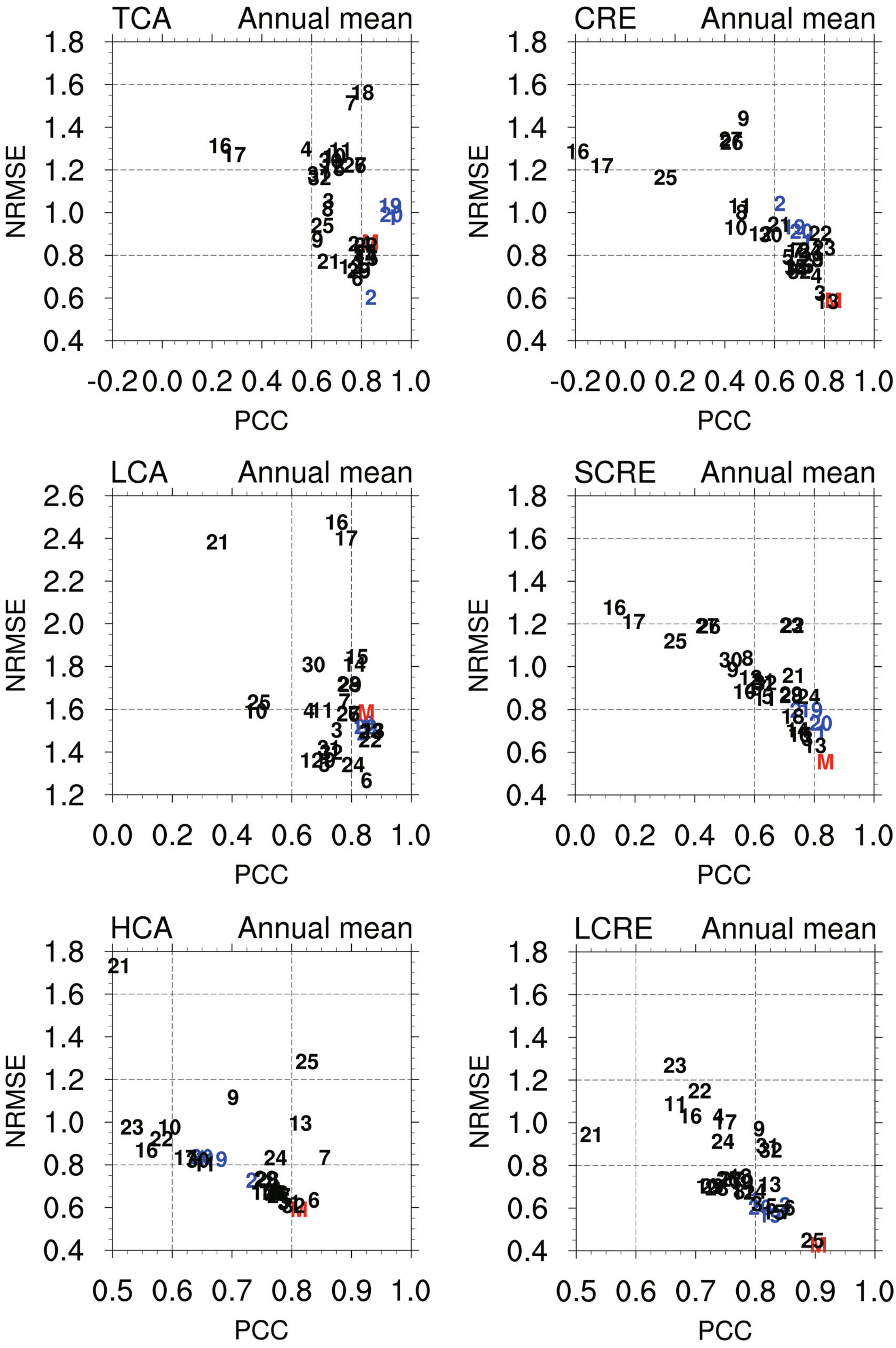

Fig. 2. The PCC (abscissa) and the domain-averaged RMSE normalized by the observed spatial standard deviation (NRMSE, ordinates) of 32 models (marked by the model number in Table 1) and the MME (marked by "M") for the TCA (%), LCA (%), HCA (%), net CRE (W m^{-2}), SCRE (W m^{-2}), and LCRE (W m^{-2}). The analysis domain is (60°S–60°N, 180°W–180°E). The best four models selected in this study are marked in blue. Note that LCA has a different *y*-axis compared to the other variables.

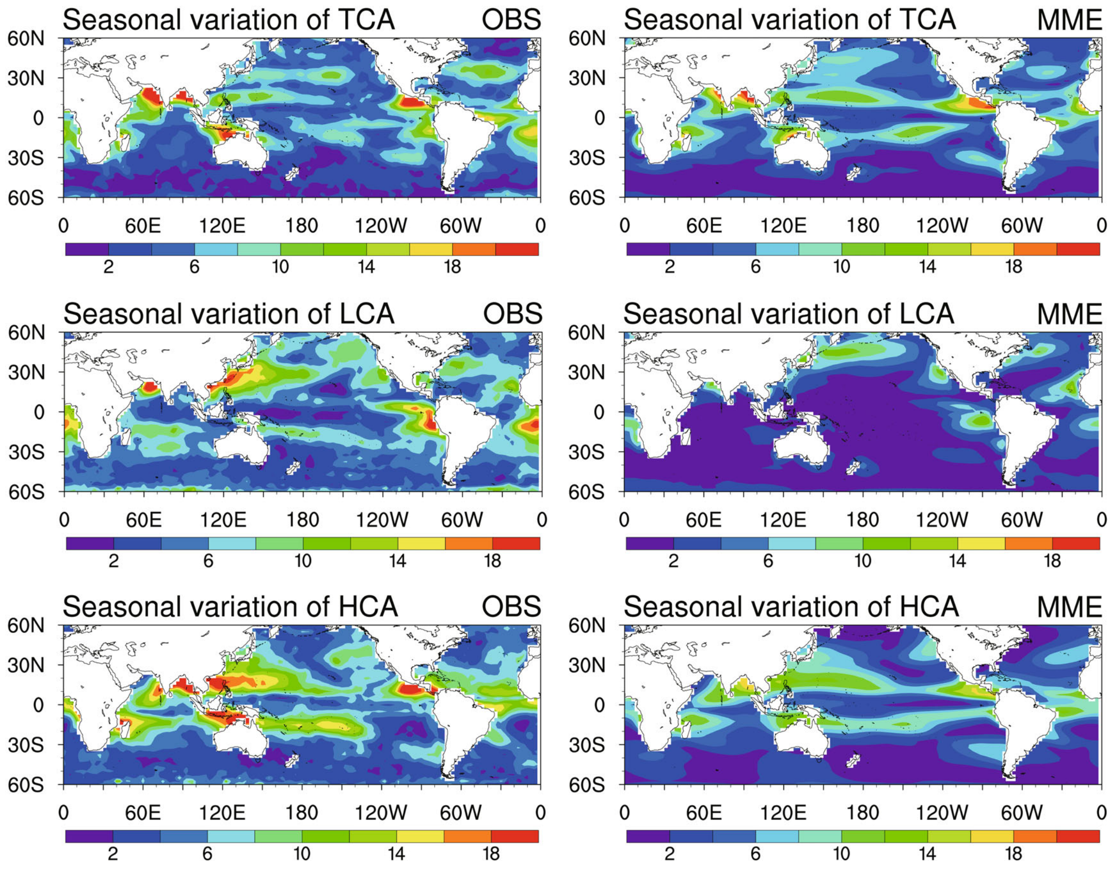

Fig. 3. Comparison of the seasonal variation of TCA (%), LCA (%) and HCA (%) between observations (ISCCP) and the MME of 32 CGCMs for the period 1984–2005.

to reduce LTS, which is favorable for the dissipation of low cloud, as suggested by the modeling study of Wyant et al. (1997). The HCA shows opposite correlation to that of LCA. As a result, the correlation of TCA with LTS is positive in the subtropical oceans, with prevailing low cloud, and negative in the equatorial convection regions, with prevailing deep convective high cloud. The MME captures the observed spatial extent and strength of the TCA response to LTS quite well—for example, the negative correlation in the equatorial Pacific and the eastern India Ocean, and the positive correlation in the eastern subtropical oceans. However, the MME produces an overly weak strength of the LCA response to LTS in the western Pacific and SPCZ, and confines the extent of the HCA response to LTS to the lower latitudes, compared to the observation. We note that ACCESS1.0, ACCESS1.3, CCSM4, GFDL-ESM2M, HadGEM2-CC, and HadGEM2-ES are again somewhat better than other models in terms of the strength of the correlation and its resemblance in the spatial pattern with the observed.

The relationship between SLP and each cloud type is examined in Fig. 7. Local SLP is regarded as the strength of large-scale subsidence. George and Wood (2010) suggested that SLP also plays an important role in modulating LCA. The observed TCA shows a negative correlation with SLP throughout the tropical and subtropical oceans, with a maximum value of around 0.6 in the western Pacific. It also shows significant positive correlation over the eastern subtropical oceans. Although the MME reproduces the relationship between SLP and HCA over the western Pacific and Indian Ocean fairly well, it is less realistic in capturing the positive correlation between LCA and SLP over the eastern subtropical oceans. Regarding the simulation by individual models, some models (e.g., CCSM4 and GFDL-ESM2M) are overly weak in reproducing the negative correlation in the western Pacific (not shown). On the contrary, ACCESS1.0, ACCESS1.3, HadGEM2-CC and HadGEM2-ES tend to overestimate the positive correlation in the subtropical and equatorial eastern Pacific.

We further examined the impacts from other variables, such as relative humidity and surface wind speed, on the interannual variability of the cloud amount, but little correlation was found (not shown).

3.4. *Best model selection*

In order to summarize the results from Figs. 5–7, and compare the model performance in a quantitative way, we calculate the spatial correlation for the area (60°S–60°N, 180°W–180°E) between two correlation maps—that of the observed correlation between TCA and large-scale variables, and that of the simulated correlation from each model (Fig.

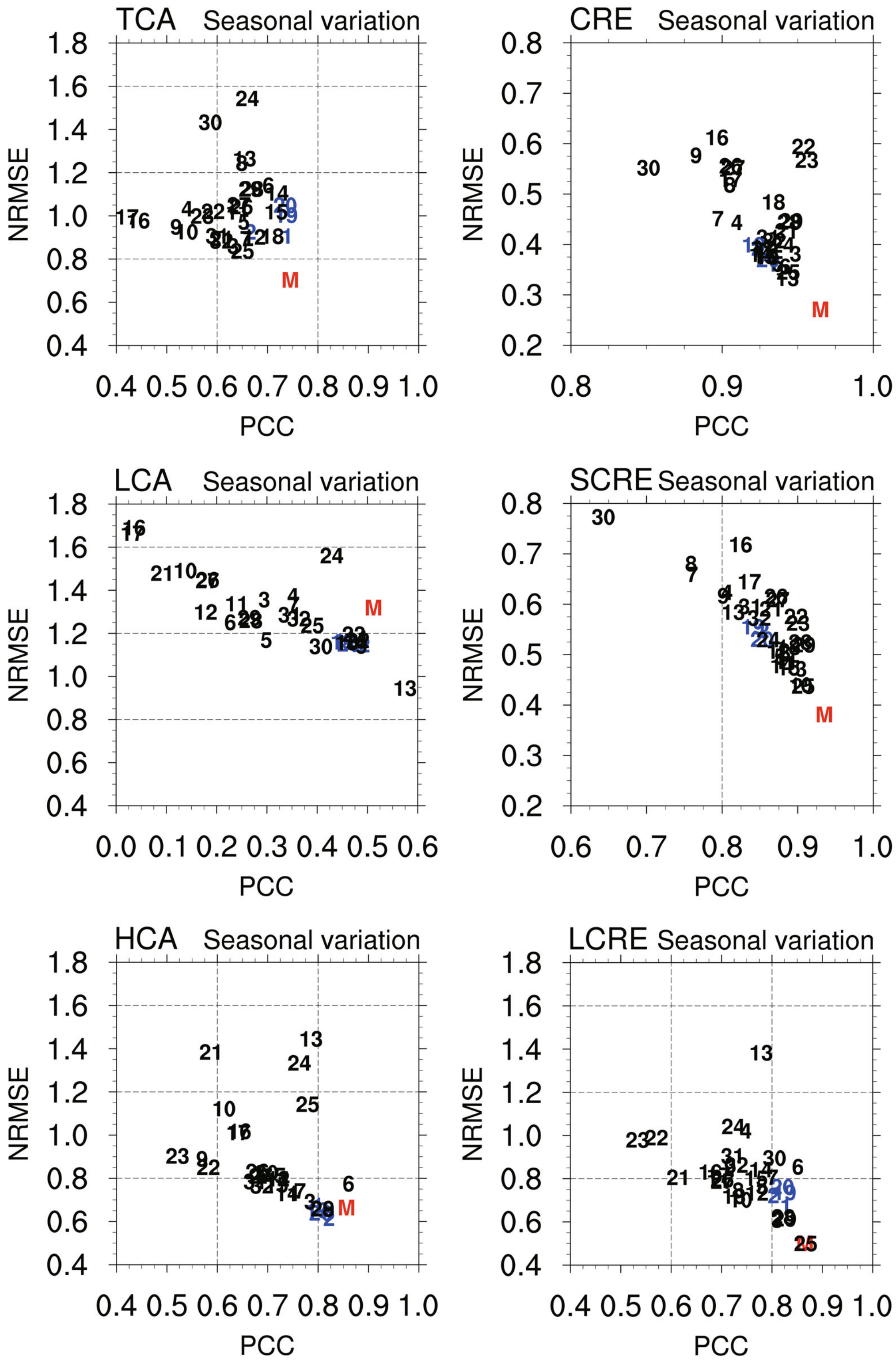

Fig. 4. As in Fig. 2 except for the seasonal standard deviation patterns for each variable. The best four models selected in this study are marked in blue.

8). While most models reproduce the spatial pattern of the cloud response to the change in meteorological variables poorly, the MME and eight models—ACCESS1.0, ACCESS1.3, CCSM4, GFDL-ESM2M, HadGEM2-CC, HadGEM2-ES, MIROC5, and MPI-ESM-P—show better skill, with PCCs over 0.55, for all large-scale variables. Note that higher correlation in this respect does not necessarily suggest the modeled cloud variation is more realistic and with

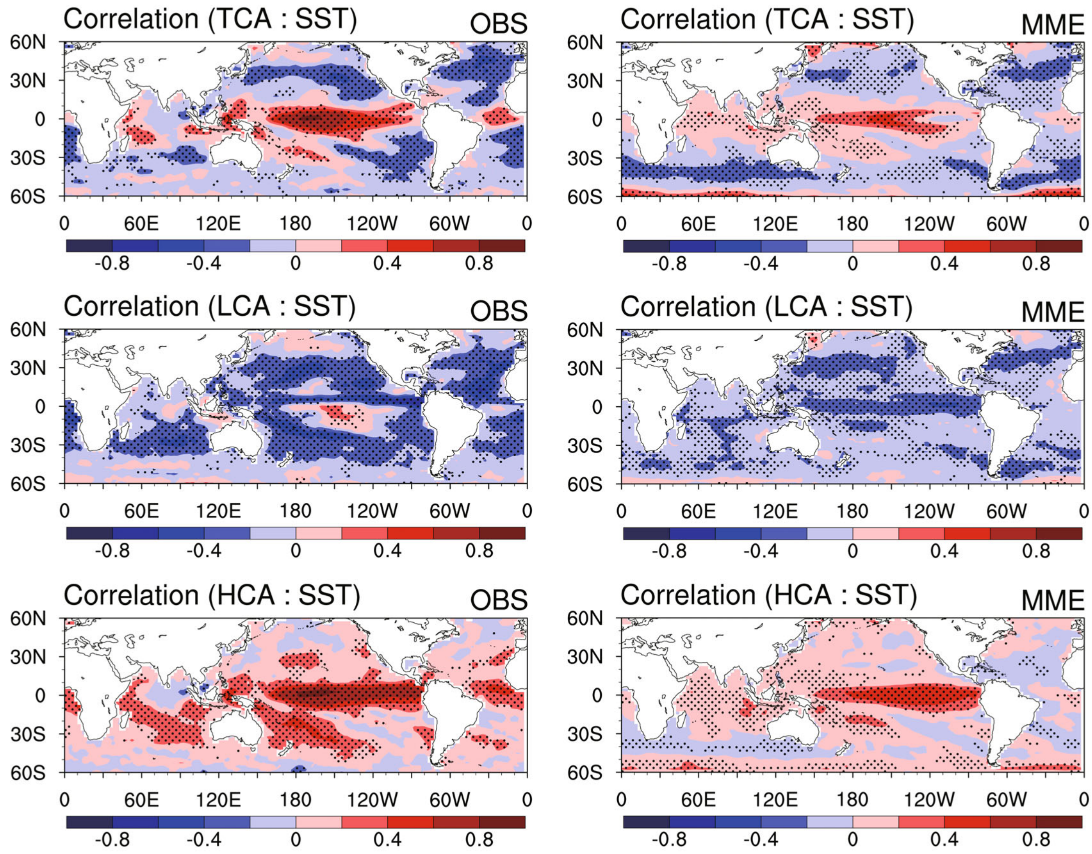

Fig. 5. Correlation between the observed SST (UK Met Office HadISST1) and (upper) TCA, (middle) LCA, and (bottom) HCA. Left-hand panels show the observed cloud (ISCCP) and right-hand panels the MME (32 models) cloud amount, and the SST anomalies are monthly anomalies relative to the long-term monthly means. Stippling indicates significance at the 99% level.

a more realistic magnitude. Among those eight models, four of them—ACCESS1.0, ACCESS1.3, HadGEM2-CC, and HadGEM2-ES—commonly show better PCC and NRMSE scores in their annual-mean patterns (section 3.1), and their amplitude patterns of annual cycles (section 3.2). Although CCSM4, GFDL-ESM2M, MIROC5 and MPI-ESM-P show comparable pattern correlation skill, they are unable to reproduce the observed LCA response in the eastern subtropical oceans.

Low cloud is the major contributor to the CRE, particularly the reflection of shortwave radiation in the marine stratocumulus regions of the eastern subtropical oceans. After selecting four areas of prevailing low cloud (black box in Fig. 1), we compare the area-averaged correlation coefficients between TCA (mostly LCA in those regions) and each large-scale variable of SST, LTS and SLP across the model simulations (Fig. 9). The observed cloud amount shows negative correlation with SST, and positive correlation with LTS and SLP. Again, ACCESS1.0, ACCESS1.3, HadGEM2-ES and HadGEM2-CC are the realistic models for the observed relationship between cloud amount and large-scale variables.

Ultimately, we choose the four best models as ACCESS1.0, ACCESS1.3, HadGEM-CC and HadGEM-ES, based on the validation metrics presented above. In fact, the MME of these four models shows better skill than the MME of all 32 models. The observations show a net radiative cooling by clouds at the top of the atmosphere of -32.7 W m^{-2}, which is the sum of longwave warming (27.3 W m^{-2}) and shortwave cooling (-60.1 W m^{-2}). The observed TCA is around 71.0%. The four best models (B4MME, hereafter) agree well with the observations in magnitude, with -24.04, -52.5 and 28.4 W m^{-2} for the net CRE, SCRE and LCRE, respectively, and 60.4% for the cloud amount. The B4MME also produces the smallest RMSE and the highest PCC for the annual-mean TCA and the amplitude in the annual variation of the cloud amounts and the CREs.

4. Future change in CREs by global warming

In this section, we discuss the possible future changes in clouds and their impact on climate, by comparing the simulations between the historical run (1950–99) and the RCP4.5 run (2050–99) using the B4MME models chosen in the previous section. The primary goal is to understand how the cloud radiative feedback will operate in a future global warming scenario, because current GCMs are diverse in their results

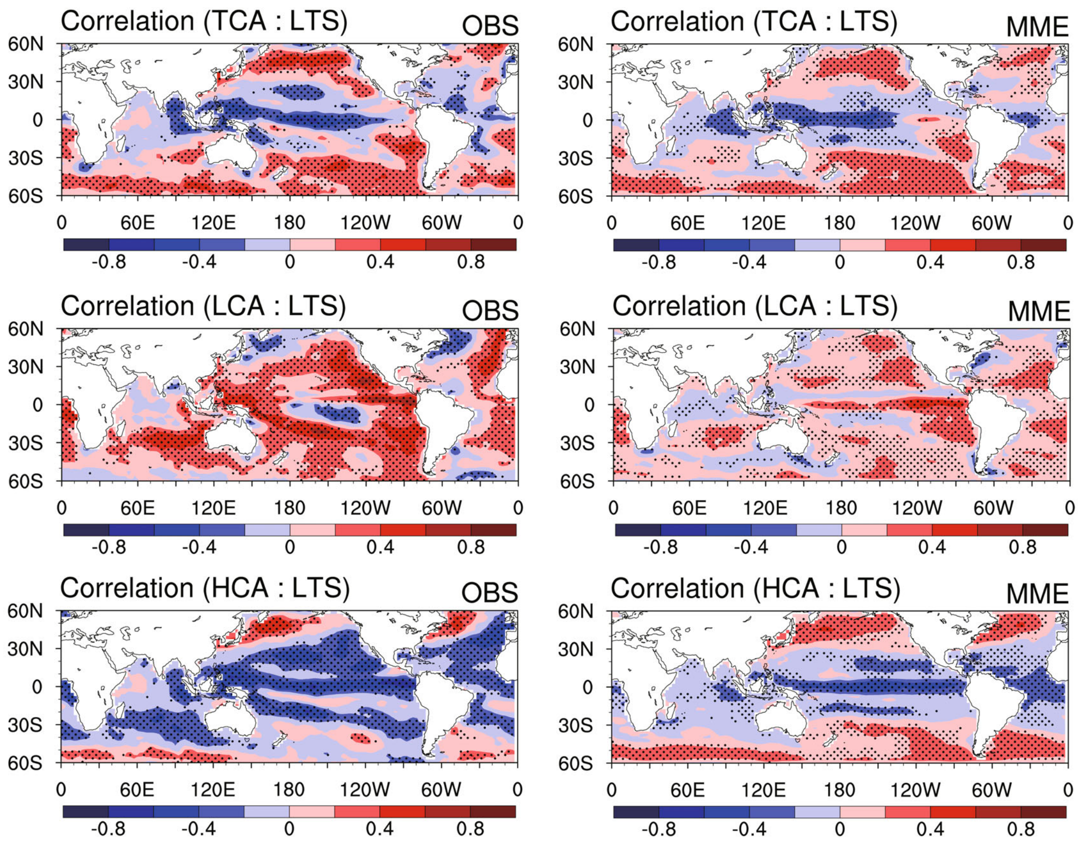

Fig. 6. Correlation between LTS and (top) TCA, (middle) LCA, and (bottom) HCA. Left-hand panels show the observations and the right-hand panels show the MME of 32 CGCMs.

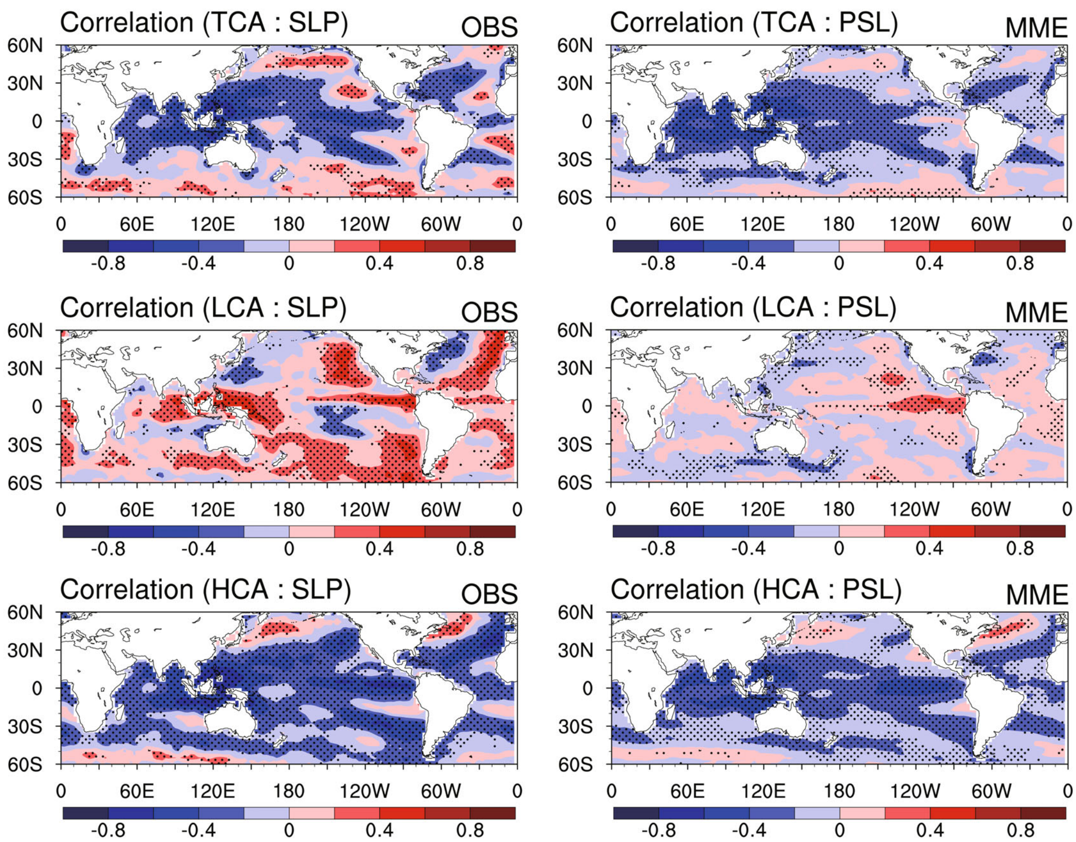

Fig. 7. As in Fig. 6 but for SLP.

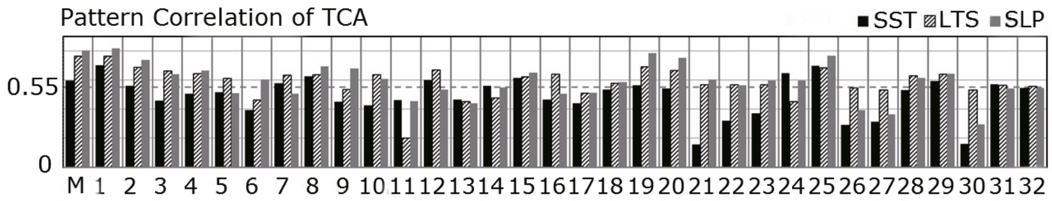

Fig. 8. PCCs between the observed and the model-simulated patterns for the serial correlations between TCA and the large-scale variables in their interannual variations. Each coefficient is averaged over the ocean area of 60°S–60°N (latitude) and 180°W–180°E (longitude). Each number indicates the model identification number in Table 1.

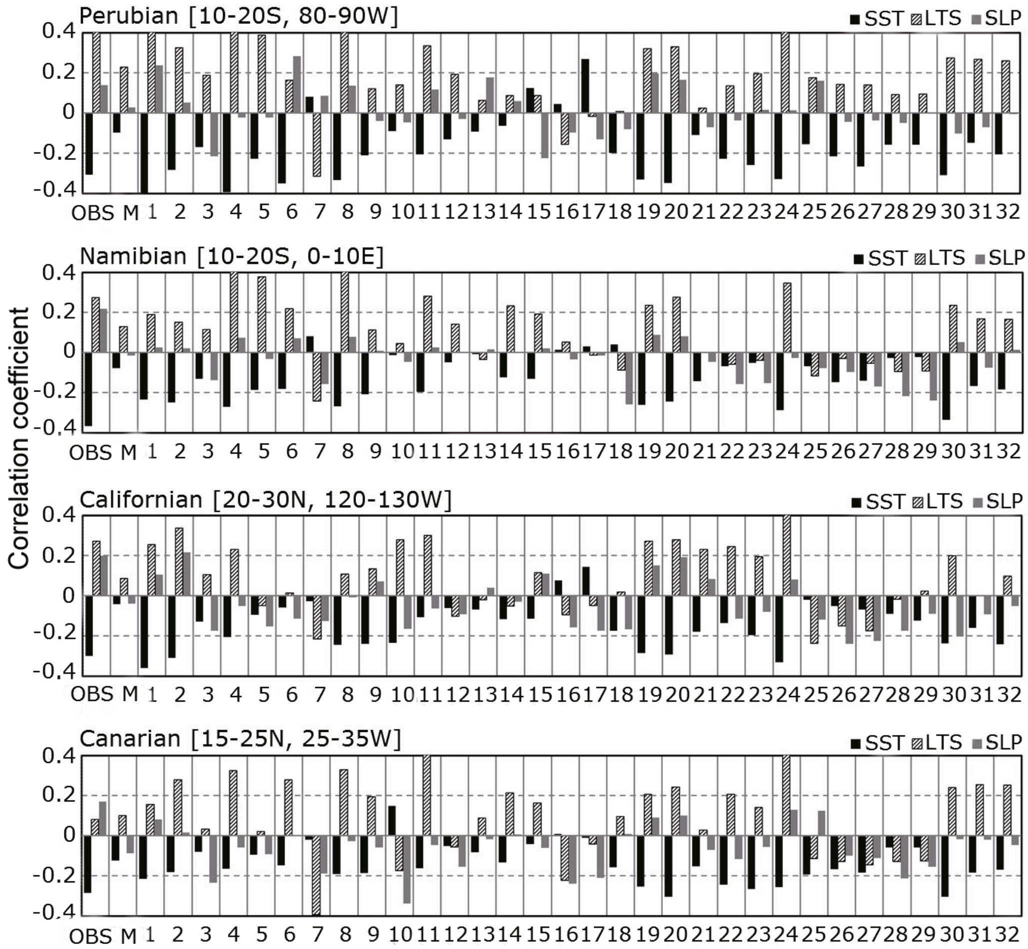

Fig. 9. Comparison of the correlation coefficient between TCA and the large-scale variables of SST (black bars), LTS (slashed bars), and SLP (gray bars) for the observation, MME, and 32 individual models. Four marine regions in Fig. 1 are compared separately.

when simulating the cloud radiative feedback, even with different signs of change. Figure 10 shows the global-mean changes in SST, TCA, LCA and CRE projected by various CGCMs, where the values indicate the areal mean over (60°S–60°N, 180°W–180°E). The magnitude of SST change varies across the simulations between 1 and 2 K, where INM-CM4.0 shows the minimum and GFDL CM3 the maximum among the models. All models project warming in response to the increase in greenhouse gases, but the degree of warming depends on the model simulation. Note that the sign and the magnitude of the CRE change also vary depending on the model. Almost half of the models show negative CRE changes (i.e., negative contributions to the SST warming), whereas the remaining models show positive changes. In general, the models that project a higher degree of SST warming show a greater increase in the net CRE. This is largely induced by the larger reduction in cloud amount and the decrease in planetary albedo. Note that this relationship might

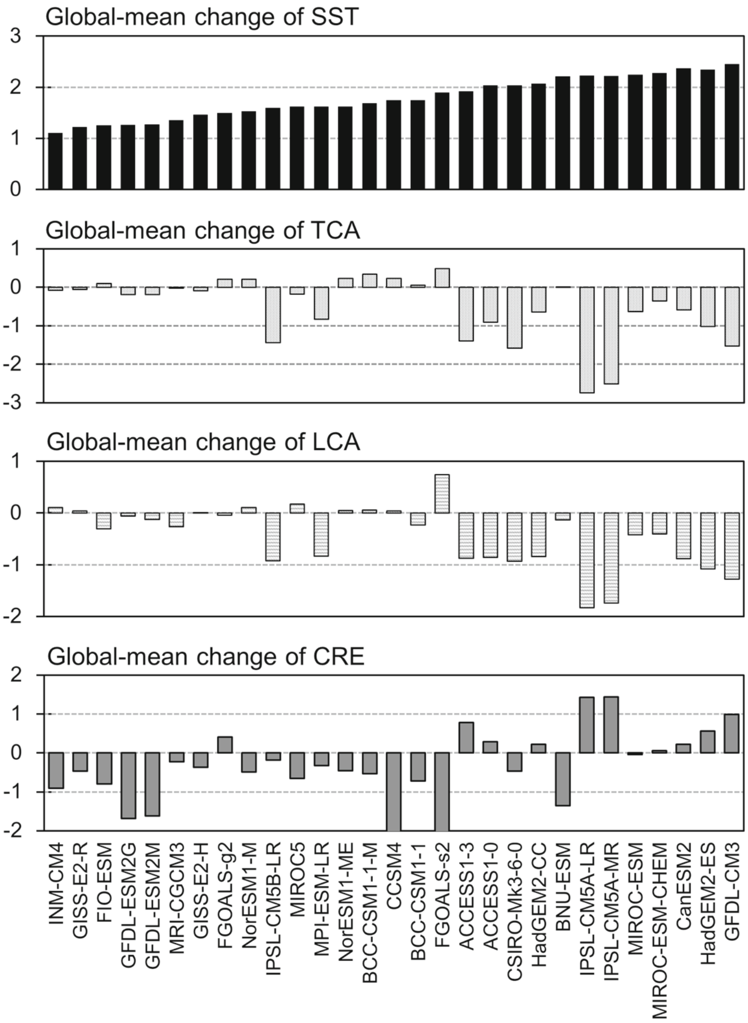

Fig. 10. Global-mean changes in SST, TCA, LCA and CRE according to 32 CGCMs. Change is defined as the departure of the global mean of 2050–99 in the RCP4.5 runs from the global mean of 1950–99 in the historical runs. Global mean here is defined as an average over (60°S–60°N, 180°W–180°E). The actual values are divided by the surface temperature increases, which are different among the models, to give the units W m^{-2} K^{-1} for the fluxes, and % K^{-1} for the cloud cover.

be altered by other climate feedbacks, which tend to complicate the relevant processes. For example, GFDL CM3 exhibits the highest SST warming, whose magnitude is comparable to those of the IPSL models (IPSL-CM5A-MR, IPSL-CM5A-LR), but it does not show the highest reduction in TCA and CRE change.

Figure 11 compares the spatial distributions of the change in TCA, LCA, CRE and SST between MME and B4MME. The stippled areas show the regions of statistical significance, where the magnitude of change exceeds one standard deviation of the intermodel spread. B4MME projects a significant decrease in TCA over most areas of the subtropical oceans, especially over the Northern Hemisphere, whereas it projects an increase in the equatorial Pacific, Atlantic Ocean and the equatorial southeastern Pacific. The changes are more prominent over the eastern basins than over the western ones, which is mainly due to the changes in LCA. The changes in TCA correspond well to the changes in the CRE. Reduced TCA occurs off the west coast of North America, with the local maximum in SST change. On the contrary, increased cloud amount (both TCA and LCA) is seen off the west coast of South America, which is accompanied by the smallest SST increase. In general, the spatial patterns of change in cloud amount and CRE correspond well with the pattern of SST change, and this supports the results from the global averages in Fig. 10. The increase in SST warming is largely associated with the large reduction in LCA off the west coast of North America and the eastern equatorial Pacific, contributing to an increase in the CRE (warming). The increased TCA in the equatorial Pacific can be understood as an increase in HCA.

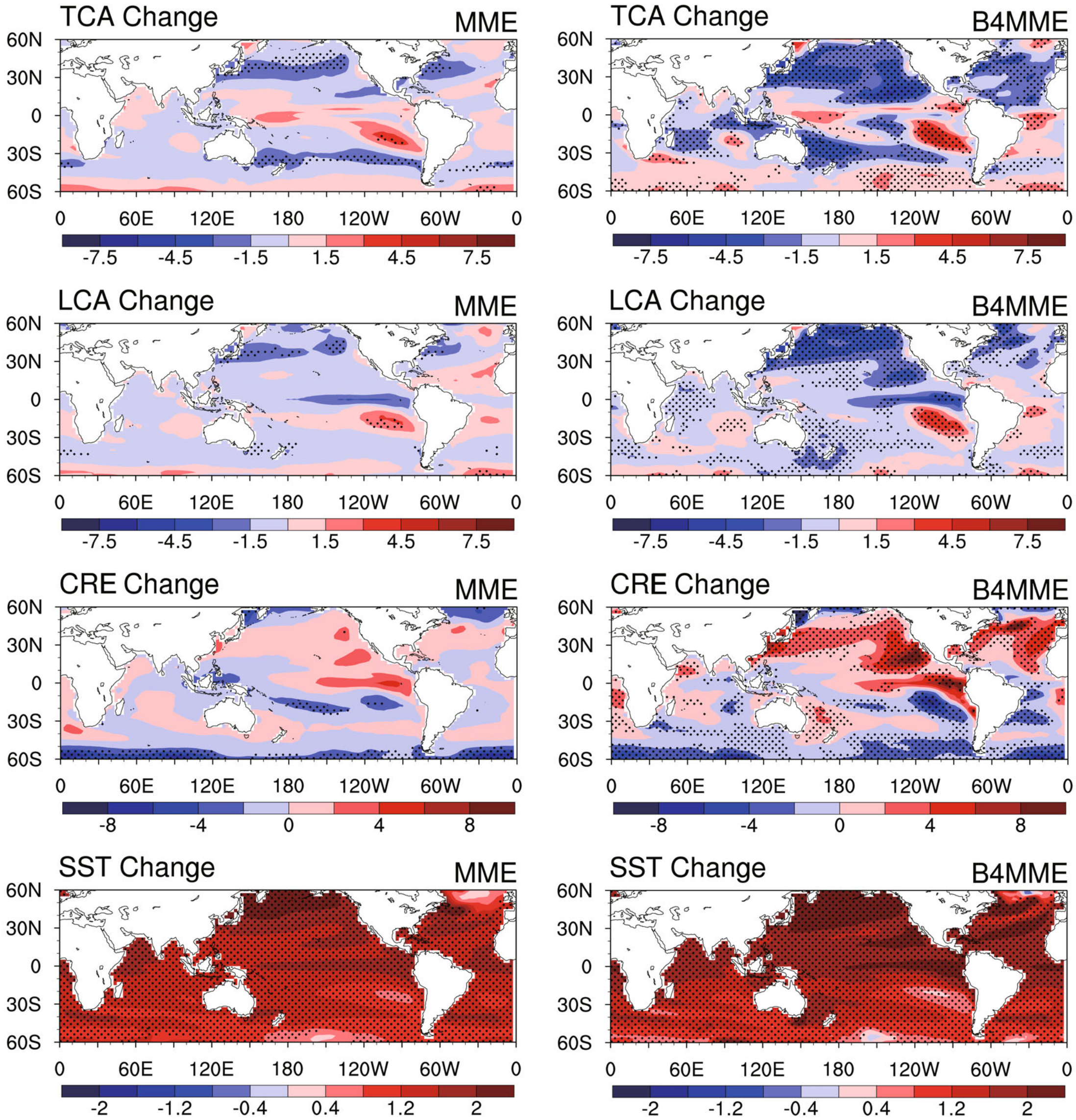

Fig. 11. Changes in total cloud cover (TCA), low cloud cover (LCA), CRE and SST for the MME and B4MME. Changes are given for the RCP4.5 simulation for the period 2050–99 relative to the historical simulation for the period 1950–99. Stippling denotes areas where the magnitude of the ensemble mean exceeds the standard deviation of intermodel spread.

Note that the spatial distribution of the projected changes by the MME is similar to that by the B4MME, although the former shows a more uniform SST pattern due to the multimodel average.

Next, we evaluate the cloud-radiative feedback (i.e., the CRE change) in future climates. Figure 12 shows the CRE changes for the MME, B4MME, and four individual models, separately. Here, we divide the CRE changes by the projected global average of SST change in each model for evaluating the cloud radiative feedback by the same SST increase. The four best models exhibit quite good agreement in their projected cloud effect changes, with negative signs in the longwave radiation and positive in the shortwave radiation. All models exhibit a warming effect (i.e., positive change in the net CRE) induced by the decrease in TCA, mainly by the reduction in LCA. This suggests positive feedback by cloud, where the low cloud reduction plays a dominant role in the warming of future climate. Note that the MME of the 32 models exhibits much smaller reductions in cloud amounts, and weaker changes in the SCRE. This results in negative feedback by cloud (i.e., negative change in the net CRE), which is in fact opposite in sign to the result from the B4MME.

5. Transient trends

This section discusses the transient trend of clouds and their impacts on climate. Figure 13 compares the anomaly

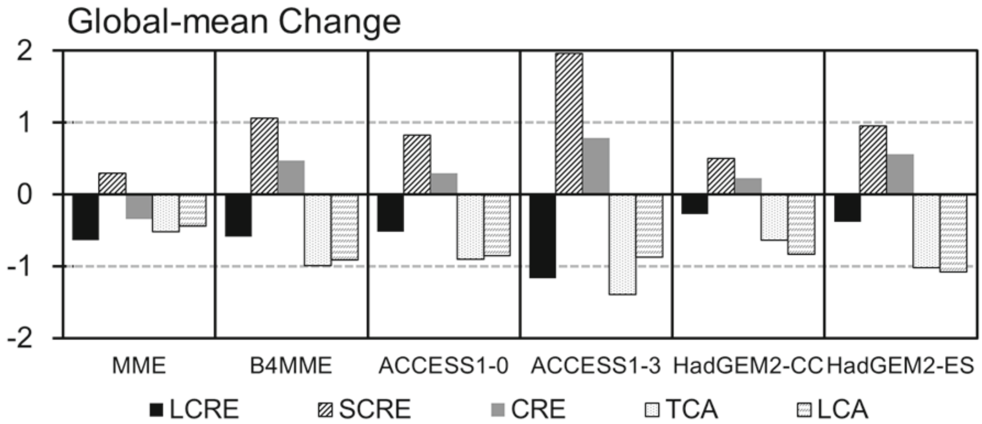

Fig. 12. Changes in the cloud radiative forcing in the LCRE, SCRE, net CRE, TCA and LCA. The actual values are divided by the surface temperature increases, which are different among the models, to give the units W m^{-2} K^{-1} for the fluxes, and % K^{-1} for the cloud cover. Each value is averaged over the ocean area of (60°S–60°N, 180°W–180°E).

time series for the global and multimodel average of the TCA, CRE and SST for the period 1901–2100, combining the simulation data from the historical runs and the RCP4.5 future scenario runs. The anomalies are departures from the climatology defined from 1901 to 1950. The shading in different colors indicates the model spread of 29 models (pink), and of the best four models (blue). The B4MME shows a decreasing trend in TCA, with a rapid decreasing trend in future climate. The global mean cloud anomaly reaches approximately −1.7% by 2100, compared against the climatology of 1901–50. The CRE shows an overall decreasing trend for the historical run period by 2005, after which there is an abrupt increasing trend in the future scenario runs. This increasing trend of the CRE corresponds to the reduction in low cloud and the shortwave cloud radiative forcing (not shown). The global-mean SST anomalies also show an increasing trend in the future, which is highly consistent with that of the CRE, suggesting a role of positive feedback by low-cloud reduction.

Individual model projections (pink) for the TCA, CRE and SST show a huge spread, even with sign changes, although the MME from the 29 models (red line) and the B4MME (blue line) show good agreement with each other in the ensemble mean time series. Despite the progress in cloud modeling in recent years, the individual models participating in CMIP5 still present diverse cloud change and feedback, with sign changes in feedbacks. It seems to be the case that most CMIP5 models cannot represent observed cloud variations, which are closely related to large-scale environmental changes.

We find that the changes in cloud differ hugely between the Northern Hemisphere and Southern Hemisphere (Fig. 13), with a more dramatic decrease in TCA in the former. The TCA in the Northern Hemisphere decreases by more than 2.0% up until 2100. On the other hand, the decreasing trend of TCA in the Southern Hemisphere is not statistically significant. The substantial reduction in TCA in the Northern Hemisphere—induced mostly by the reduction in low cloud—tends to result in the reduction of the cloud cooling effect, and thus a larger temperature increase in the Northern Hemisphere. This will drive an increase in the hemispheric thermal contrast and associated atmospheric circulation changes.

6. Summary

Using observational data and the historical simulations of 32 CMIP5 CGCMs driven by identical natural and anthropogenic forcing data, this study investigates the realism of their cloud simulations. For a systematic evaluation, this study constructs model intercomparison metrics, which include the examination of the time-mean distributions of cloud and the CRE, their monthly variations, and the interannual variations affected by large-scale environmental conditions such as SST, LTS, and SLP. In addition, using the RCP4.5 climate change simulations, where the anthropogenic greenhouse gas forcing stabilizes at 4.5 W m^{-2} after 2100, this study further investigates the degree to which clouds could change and how cloud feedback might contribute to global warming.

Based on observation using ISCCP cloud data and atmospheric reanalysis data, we find that the interannual variation of LCA is associated with that of LTS. This is in turn closely tied to the SST and SLP changes; that is, large-scale subsidence. Clouds at different heights show sign changes in correlation with SST: high (low) clouds have a positive (negative) correlation with SST. In addition, the correlation patterns between the TCA and the large-scale fields clearly separate the tropical convective regime and subtropical subsidence regime. The former is dominated by high cloud, while the latter is controlled by low cloud. The mechanisms for the low-level cloud variation are related in that the SST in-

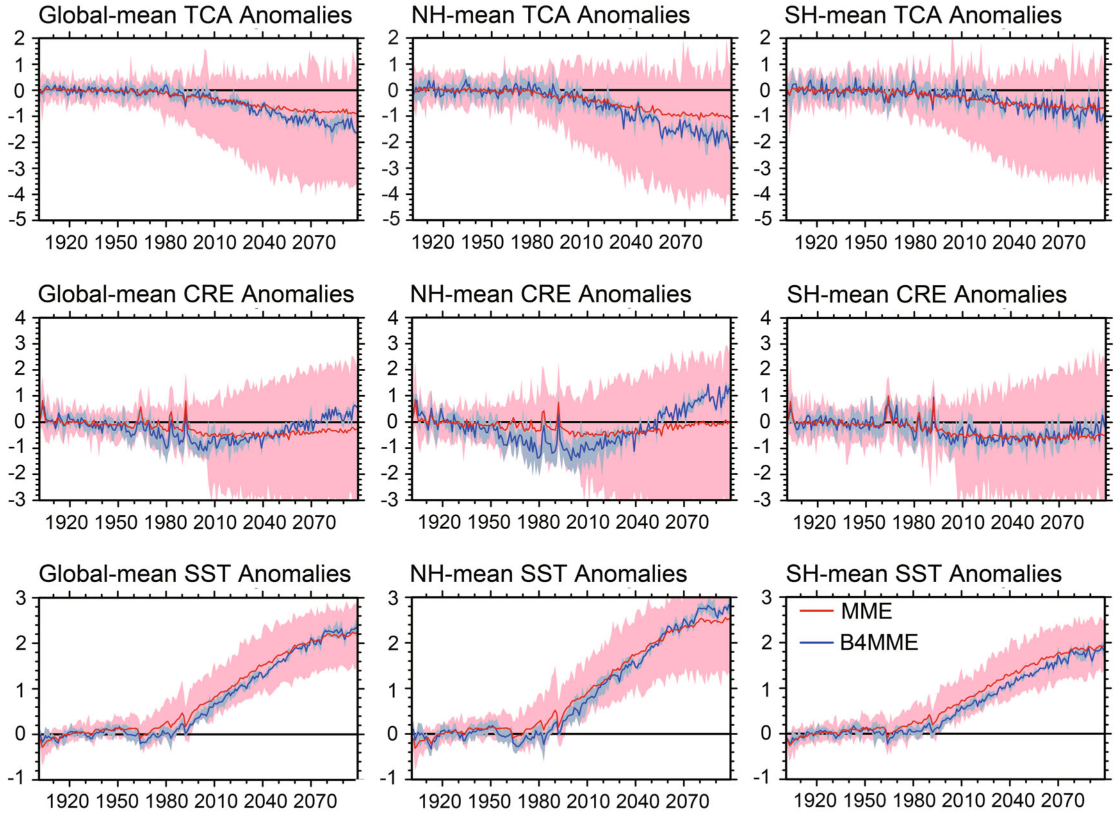

Fig. 13. Projected TCA, net CRE and SST by CGCMs. The annual mean value is averaged over (left) the range (60°S–60°N, 180°W–180°), (middle) the Northern Hemisphere (0°–60°N, 180°W–180°E), and (right) the Southern Hemisphere (60°S–0°, 180°W–180°E). All values are shown as anomalies from the 1901–50 mean. Red and blue lines indicate the MME and B4MME, respectively, and shading in pink and sky blue denotes the uncertainty range for the MME and B4MME, respectively, as assessed by individual model simulations.

crease results in the destabilization of the boundary layer and reduction of LTS, causing enhanced vertical motion within and around the cloud deck. On the other hand, the increased large-scale subsidence (i.e., higher SLP) above the cloud-topped boundary layer tends to increase the low cloud, being less affected by SST (Clement et al., 2009; Shin et al., 2014).

In general, the CGCMs show large spread in their simulation of cloud amounts and their impacts on radiation, as well as common deficiencies. The observed relationships between cloud amount and the controlling large-scale environment are also reproduced diversely by the various models. In most evaluations, the average of all model simulations (i.e., the MME) shows better skill than individual models in reproducing the observed features. This suggests a large model spread and uncertainty in cloud simulation, which is substantially canceled out by the MME. Through scoring based on PCCs and NRMSEs for the annual mean cloud distribution and their amplitudes in monthly variation, and for the correlation patterns for cloud amount and controlling large-scale variables on the interannual time scale, this study selected four models—ACCESS1.0, ACCESS1.3, HadGEM-CC and HadGEM-ES. The average of these four models (the B4MME) demonstrates higher skill for the cloud evaluation metrics than the MME.

By comparing the RCP4.5 runs and historical runs, this study further addresses the possible future changes in cloud and CREs simulated by CMIP5 CGCMs. All models evaluated in this study project the SST warming due to the increase in greenhouse gases in the future climate, but the magnitude of the SST warming shows substantial intermodel differences. The magnitude of the CRE change is also diverse among models, even with different signs of change. In general, the models that project a higher degree of SST warming show a greater increase in the net CRE. This is largely induced by the larger reduction in cloud amount and the decrease in planetary albedo. In the future climate projection, the four selected best models show good agreement with one another in terms of their reduction in low cloud, suggesting a positive feedback role to global warming. It is also found that the change is asymmetric between the hemispheres, with the change in the Northern Hemisphere being greater than that in the Southern Hemisphere.

In modeling future climate, the CMIP5 models are still quite diverse in simulating the cloud feedback, even varying in the sign of feedback. This seems to be largely due to the poor representation of low cloud variation and the controlling processes of the large-scale environmental conditions in most models. The average of the best models tends to reduce the bias in cloud and CRE simulations substantially. Their simulations for future climate change are also robust and consistent across them, generating more confidence in their projections compared with the average of all models. This study suggests a more comprehensive method for testing the realism of cloud simulations in current climate models, and addresses how much the model uncertainty can be reduced by selecting the best models.

Even though we admit the satellite simulator is an ideal tool to diagnose cloud radiation interaction (e.g., Zelinka et al., 2012a, 2012b; Klein et al., 2013), this study compares the cloud amount diagnosed in each model based on their own cloud diagnostic assumptions and vertical overlapping, which is different across the models. This is an inevitable choice, as the satellite simulator data are not available for every CMIP5 participating model. Comparison based on the satellite simulator is a whole new avenue of research, and is well beyond the current scope of this study. Further studies in the context of satellite simulators should be conducted in the future.

Acknowledgements. The authors thank Joel NORRIS for providing the adjusted ISCCP data. The CMIP5 data were obtained from the data archive (http://cmip-pcmdi.llnl.gob/cmip5/index.html). This research was supported by the APEC Climate Center. ML and DK were supported by the UNIST research fund (Grant No. 1.09006.01). Additional support was provided by a grant (Grant No. 14AWMP-B082564-01) from the Advanced Water Management Research Program funded by the Ministry of Land, Infrastructure and Transport of the Korean government.

REFERENCES

Andrews, T., J. M. Gregory, M. J. Webb, and K. E. Taylor, 2012: Forcing, feedbacks and climate sensitivity in CMIP5 coupled atmosphere-ocean climate models. *Geophys. Res. Lett.*, **39**(9), L09712, doi: 10.1029/2012GL051607.

Bony, S., and J.-L. Dufresne, 2005: Marine boundary layer clouds at the heart of tropical cloud feedback uncertainties in climate models. *Geophys. Res. Lett.*, **32**(20), L20806, doi: 10.1029/2005GL023851.

Bony, S., and Coauthors, 2006: How well do we understand and evaluate climate change feedback processes? *J. Climate*, **19**, 3445–3482.

Clement, A. C., R. Burgman, and J. R. Norris, 2009: Observational and model evidence for positive low-level cloud feedback. *Science*, **325**, 460–464, doi: 10.1126/science.1171255.

Dufresne, J. L., and S. Bony, 2008: An assessment of the primary sources of spread of global warming estimates from coupled atmosphere-ocean models. *J. Climate*, **21**, 5135–5144.

Eastman, R., S. G. Warren, and C. J. Hahn, 2011: Variations in cloud cover and cloud types over the ocean from surface observations, 1954-2008, *J. Climate*, **24**, 5914–5934.

George, R. C., and R. Wood, 2010: Subseasonal variability of low cloud radiative properties over the southeast Pacific Ocean. *Atmospheric Chemistry and Physics*, **10**, 4047–4063, doi: 10.5194/acp-10-4047-2010.

Hartmann, D. L., L. A. Moy, and Q. Fu, 2001: Tropical convection and the energy balance at the top of the atmosphere. *J. Climate*, **14**, 4495–4511.

IPCC, 2013: Climate Change 2013: The Physical Science Basis. Working Group I Contribution to the IPCC Fifth Assessment Report (AR5). Intergovernmental Panel on Climate Change, Geneva, Switzerland.

Klein, S. A., and D. L. Hartmann, 1993: The seasonal cycle of low stratiform clouds. *J. Climate*, **6**, 1587–1606.

Klein, S. A., Y. Y. Zhang, M. D. Zelinka, R. Pincus, J. Boyle, and P. J. Gleckler, 2013: Are climate model simulations of clouds improving? An evaluation using the ISCCP simulator. *J. Geophys. Res.*, **118**, 1329–1342, doi: 10.1002/jgrd.50141.

Li, J.-L. F., D. E. Waliser, G. Stephens, S. Lee, T. L'Ecuyer, S. Kato, N. Loeb, and H.-Y. Ma, 2013: Characterizing and understanding radiation budget biases in CMIP3/CMIP5 GCMs, contemporary GCM, and reanalysis. *J. Geophys. Res.*, **118**, 8166–8184, doi: 10.1002/jgrd.50378.

Norris, J. R., and C. B. Leovy, 1994: Interannual variability in stratiform cloudiness and sea surface temperature. *J. Climate*, **7**, 1915–1925.

Pavolonis, M. J., A. K. Heidinger, and T. Uttal, 2005: Daytime global cloud typing from AVHRR and VIIRS: Algorithm description, validation, and comparisons. *J. Appl. Meteor.*, **44**, 804–826, doi: 10.1175/JAM2236.1.

Platnick, S., M. D. King, S. A. Ackerman, W. P. Menzel, B. A. Baum, J. C. Riédi, and R. A. Frey, 2003: The MODIS cloud products: Algorithms and examples from Terra. *IEEE Trans. Geosci. Remote Sens.*, **41**(2), 459–473.

Ramanathan, V. and Coauthors, 1989: Cloud-radiative forcing and climate: Results from the earth radiation budget experiment, *Science*, **243**, 57–63.

Randall, D. A., M. E. Schlesinger, V. Galin, V. Meleshko, J. J. Morcrette, and R. Wetherald, 2006: Cloud feedbacks. *Frontiers in the Science of Climate Modeling*, J. T. Kiehl and V. Ramanathan, Eds., Cambridge University Press.

Randall, D. A., and Coauthors, 2007: Climate models and their evaluation. *The Physical Science Basis*, Contribution of Working Group I to the Fourth Assessment Report of the Intergovernmental Panel on Climate Change, S. Solomon et al., Eds., Cambridge University Press, 589–662

Rayner, N. A., D. E. Parker, E. B. Horton, C. K. Folland, L. V. Alexander, D. P. Rowell, E. C. Kent, and A. Kaplan, 2003: Global analyses of sea surface temperature, sea ice, and night marine air temperature since the late nineteenth century. *J. Geophys. Res.*, **108**(D14), 4407, doi: 10.1029/2002JD002670.

Rossow, W. B., and R. A. Schiffer, 1999: Advances in understanding clouds from ISCCP. *Bull. Amer. Meteor. Soc.*, **80**, 2261–2287.

Shin, S. H., M. I. Lee, and O. Y. Kim, 2014: Examinations of cloud variability and future change in the coupled model intercomparison project phase 3 simulations. *Asia-Pacific Journal of Atmospheric Sciences*, **50**(4), 481–495.

Soden, B. J., and I. M. Held, 2006: An assessment of climate feedbacks in coupled ocean-atmosphere models. *J. Climate*, **19**, 3354–3360.

Stephens, G. L., 2005: Cloud feedbacks in the climate system: A critical review. *J. Climate*, **18**, 237–273.

Taylor, K. E., R. J. Stouffer, and G. A. Meehl, 2012: An overview of CMIP5 and the experiment design. *Bull. Amer. Meteor. Soc.*, **93**, 485–498.

Uppala, S. M., and Coauthors, 2005: The ERA-40 re-analysis. *Q. J. R. Meteorol. Soc.*, **131**, 2961–3012.

Vial, J., J.-L. Dufresne, and S. Bony, 2013: On the interpretation of inter-model spread in CMIP5 climate sensitivity estimates. *Climate Dyn*., **41**, 3339–3362.

Waliser, D. E., and Coauthors, 2009: Cloud ice: A climate model challenge with signs and expectations of progress. *J. Geophys. Res*., **114**(D8), D00A21, doi: 10.1029/2008JD010015.

Webb, M. J., and Coauthors, 2006: On the contribution of local feedback mechanisms to the range of climate sensitivity in two GCM ensembles. *Climate Dyn*., **27**, 17–38.

Wood, R., and D. L. Hartmann, 2006: Spatial variability of liquid water path in marine low cloud: The importance of mesoscale cellular convection. *J. Climate*, **19**, 1748–1764.

Worley, S. J., S. D. Woodruff, R. W. Reynolds, S. J. Lubker, and N. Lott, 2005: ICOADS release 2.1 data and products. *Inter. J. Climatol.*, **25**, 823–842, doi: 10.1002/joc.1166.

Wyant, M. C., C. S. Bretherton, H. A. Rand, and D. E. Stevens, 1997: Numerical simulations and a conceptual model of the stratocumulus to trade cumulus transition. *J. Atmos. Sci*., **54**, 168–192.

Wyant, M. C., C. S. Bretherton, J. T. Bacmeister, J. T. Kiehl, I. M. Held, M. Zhao, S. A. Klein, and B. J. Soden, 2006: A comparison of low-latitude cloud properties and their response to climate change in three AGCMs sorted into regimes using midtropospheric vertical velocity. *Climate Dyn*., **27**, 261–279.

Yeh, S.-W., Y.-G. Ham, and J.-Y. Lee, 2012: Changes in the Tropical Pacific SST trend from CMIP3 to CMIP5 and its implication of ENSO. *J. Climate*, **25**, 7764–7771.

Zelinka, M. D., S. A. Klein, and D. L. Hartmann, 2012a: Computing and partitioning cloud feedbacks using cloud property histograms. Part I: Cloud radiative kernels. *J. Climate*, **25**, 3715–3735, doi: 10.1175/JCLI-D-11-00248.1.

Zelinka, M. D., S. A. Klein, and D. L. Hartmann, 2012b: Computing and partitioning cloud feedbacks using cloud property histograms. Part II: Attribution to changes in cloud amount, altitude, and optical depth. *J. Climate*, **25**, 3736–3754, doi: 10.1175/JCLI-D-11-00249.1.

Zelinka, M. D., S. A. Klein, K. E. Taylor, T. Andrews, M. J. Webb, J. M. Gregory, and P. M. Forster, 2013: Contributions of different cloud types to feedbacks and rapid adjustments in CMIP5. *J. Climate*, **26**, 5007–5027, doi: 10.1175/JCLI-D-12-00555.1.